Composites Science and Technology 107 (2015) 113–119

Contents lists available at ScienceDirect

Composites Science and Technology

journal homepage: www.elsevier.com/locate/compscitech

Fast deflagration to detonation transition of energetic material based on a quasi-core/shell structured nanothermite composite

Zhiqiang Qiao [a], Jinpeng Shen [b], Jun Wang [a], Bing Huang [a], Zhijian Yang [a], Guangcheng Yang [a,*], Kaili Zhang [c]

[a] Institute of Chemical Materials, China Academy of Engineering Physics, Mianyang 621900, Sichuan, China
[b] Sichuan New Material Research Center, Mianyang 621000, Sichuan, China
[c] Department of Mechanical and Biomedical Engineering, City University of Hong Kong, 83 Tat Chee Avenue, Kowloon, Hong Kong

ARTICLE INFO

Article history:
Received 8 July 2014
Received in revised form 30 November 2014
Accepted 7 December 2014
Available online 12 December 2014

Keywords:
A. Hybrid composites
A. Functional composites
B. Interface
B. Thermal properties
D. Photoelectron spectroscopy (XPS)

ABSTRACT

Nanothermites (also called metastable intermolecular composites), composed of nanoscale metals and metal oxides, have drawn increasing interests as energetic materials over the past two decades. Nanothermites have twice the energy density of 2,4,6-trinitroluene, and their nanostructures, functions, energy release, and reaction performance are continuously being improved. However, these materials suffer from low pressure because of low gas expansion from the reaction and incapability of deflagration to detonation transition (DDT). Fast DDT is necessary to substantially improve the reaction velocity and output pressure not only of nanothermites but also of other monomolecular organic energetic materials, such as cyclotrimethylene trinitramine (RDX) and octogen. Accordingly, this study aims to produce energetic composites material that are safe, green, and free from heavy metals. A strategy of rapid DDT acceleration is proposed by fabricating quasi-core/shell structured materials of RDX@Fe_2O_3–Al based on Fe_2O_3–Al nanothermites. A surface modifying and ultrasonic synthesis technology is also demonstrated. Scanning electron microscopy and X-ray photoelectron spectroscopy characterizations prove that the material comprises an RDX core and an Fe_2O_3–Al nanothermite shell. Results of closed vessel combustion tests show that the RDX@Fe_2O_3–Al combustion velocity accelerates to an average pressurization rate of 2.527 MPa/μs. DDT tube tests further confirm that DDT accelerates to a primer explosive level in which the run-to-detonation distances of DDT is below the test-condition limitation (<15 mm). Sensitivity tests also reveal that the RDX@Fe_2O_3–Al composite has low sensitivity to impact, friction, and electric spark. Therefore, the RDX@Fe_2O_3–Al composite with a quasi-core/shell structure is a potential green and safe fast DDT energetic material that is easy to synthesize and applicable to other quasi-core/shell structures.

1. Introduction

Nanothermites (also known as metastable intermolecular composites, MIC), composed of a metal fuel and a metal oxide in nanoscale, are attracting significant interest over the last two decades. The reaction kinetics of nanothermite could be significantly improved because of the drastic heat reduction and mass transfer distances in the nanoscale level, leading to several attractive properties, such as low ignition/onset-reaction temperature, high combustion velocity, and self-propagation in the microscale [1–4]. Several potential MIC applications [5–10] have been proposed using nanothermites as energetic materials. In the recent two years, increasing number of studies on nanostructures, such as hollow nanosphere [11], nanowire [12], core/shell nano-arrays [13], and assembly nano-particles [14,15] have been demonstrated to improve the MIC performances, especially the various designs that have been proposed to improve the MIC combustion velocity or pressurization [16–19]. However, to the best of our knowledge, the attained MIC combustion wave speeds are not significantly high and only exhibit a maximum value of 2500 m/s for Bi_2O_3–Al MIC [20]. One key reason causing this limitation is that minute gas products are generated during MIC combustion, which is the key role of mass and heat transfer under turbulent flow [21]. Evidently, the lack of high pressure during an MIC reaction is a key limitation that could be used for various applications, such as initiation, deflagration to detonation transition (DDT), and driving metal. Compared with MIC, several monomolecular organic energetic materials, such as cyclotrimethylene trinitramine (RDX) and octogen (HMX), are superior because of the resulting high

* Corresponding author. Tel.: +86 812 2485072.
E-mail address: ygcheng@caep.ac.cn (G. Yang).

http://dx.doi.org/10.1016/j.compscitech.2014.12.005
0266-3538/

pressure gases during combustion or detonation. RDXs have been the most commonly used high explosives in mining and military applications. However, their combustion velocities are considerably slow (less than 10 m/s) despite of their detonation velocity of more than 8000 m/s. Moreover, realizing DDTs is difficult unless intense confinement and large amounts of charge are available.

For energetic materials use, DDT is the key process to improve the reaction velocity and output pressure because of the difference between combustion and detonation. The former only offers the weak pressures and combustion waves, and the latter offers extremely high pressures and shock waves. To initiate the high explosive charge, primer explosives (PEs), such as lead azide, lead styphnate, and cadmium carbohydrazide perchlorate, are generally used to attain a rapid DDT and output shock wave. These PEs contain lead or other heavy metal elements, and therefore are mostly hypertoxic and cause substantial harm to the environment and human health [22]. For example, a survey showed that lead in the blood of an employee working in an FBI shooting range in America was ten times that of the U.S. Federal Government standard [23]. In recent years, several green explosives, such as high-nitrogen [24,25], azides [26], nitrogen-rich heterocyclic compound, and their salts [27–30] have been synthesized as potential PEs. However, organic wastewater and other pollutant are still difficult to mitigate during the manufacture of these materials. Furthermore, most of these materials are extremely sensitive to random stimulations, such as impact, friction, and electro-static discharge, which may easily cause accidental explosion and severe damage during manufacturing, transport, and usage. Compared with PEs, several high explosives (RDX and HMX) and MIC are more environment-friendly and less sensitive to impact, friction, and electric spark (ES). These characteristics make them attractive candidates for PEs. However, significant challenges in DDT acceleration must be overcome to realize the transition by themselves.

Core/shell structure has been an effective means to improve performance of the composites materials by combining the unique characteristics of core materials and shell materials in recent years [31–33]. In this study, a strategy was proposed by fabricating a novel quasi-core/shell structure material RDX@Fe_2O_3–Al based on Fe_2O_3–Al nanothermites to accelerate the DDT of MIC and high explosives. The main underlying principle of these methods is that RDX particle surfaces are enwrapped with Fe_2O_3–Al nanothermites, forming a quasi-core/shell structure. Thus, the RDX surface in the core could be ignited to burn through the fast MIC combustion, thereby accelerating the RDX. In addition, the high pressure and gases produced through RDX would accelerate the MIC heat and mass transfer in shell, thereby accelerating the RDX. To obtain the abovementioned quasi-core/shell structure material (RDX@MIC), a surface modifying and ultrasonic process are demonstrated. In addition, further combustion, DDT, and sensitivity tests are performed to prove the superiorities of the synthesized materials.

2. Experimental section

2.1. Materials, synthesis, and characterization

To determine the particle size effect, two types of RDXs were used in the present study. Recrystallized RDX (R-RDX) particles and fine RDX (F-RDX) were purchased from Yinguang Chem. Co., Ltd. Al nanoparticles with an average diameter of 100 nm, having a ~5 nm oxide shell and active metal content of 65.0 wt.% were purchased from Wuhan Nanoparticle Co., Ltd.

For green purpose and nanothermite use, Fe_2O_3 nanoparticles were synthesized through sol–gel method and low-temperature CO_2 supercritical extraction (SCE) process as describe in Ref. [34]. About 10.0 g of $Fe(NO_3)_3{\cdot}9H_2O$ was dissolved in 10.0 g of anhydrous ethanol to give a clear red–orange solution. Upon adding 2.0 g of propylene oxide into the solution with stirring, the solution color changed to dark red–brown. By maintaining the solution at 45 °C, gelation occurred in less than 5 min. After aging the gel at 45 °C for 24 h, anhydrous ethanol was then added in the solution and replaced every 24-h period for 3–5 times. The CO_2 SCE process was subsequently performed in a vessel where the liquid in the pores were exchanged with liquid CO_2. After CO_2 exchanging, the vessel temperature increased to 45 °C and its pressure reached 15 MPa. The aerogel was obtained by maintaining the temperature and pressure for 1 h followed by depressurization. To remove the organic impurity, the aerogel was heated in a muffle furnace at 350 °C for 3 h, and then the Fe_2O_3 nanoparticles were obtained.

Fig. 1 shows that the RDX@Fe_2O_3–Al quasi-core/shell structure was synthesized via a similar surface modification and ultrasonic approach. In addition, this method is similar to that reported in the literature [35]. First, R-RDX or F-RDX raw materials were modified using estane. About 0.512 g of Estane was dissolved in 20 mL of dichloroethane ($C_2H_4Cl_2$) at 50 °C to form a colorless transparent solution. After allowing the solution to naturally cool to room temperature, 20 g of R-RDX (or F-RDX) was added to the and the mixture was stirred for 30 min. The modified R-RDX or (or F-RDX) microparticles were obtained through vacuum filtration and dried in an oven at 60 °C for 6 h. Second, the modified R-RXD (or F-RDX), Al, and Fe_2O_3 nanoparticles were ultrasonicated to form quasi-core/shell structures. Exactly 3.84 g of Al and 6.16 g of Fe_2O_3 were dispersed into 100 mL of isopropanol with ultrasonic irradiation at output acoustic power of 240 W and frequency of 40 kHz (Jeken Ultrasonic Cleaner PS-40, China) for 60 min. Moreover, a given quality of estane-modified R-RDX (or FRDX) particles were dispersed into 40 mL of isopropanol, facilitated by using the other ultrasonic apparatus (Model KQ-500VDE, 100 kHz, 500 W, and 40% power intensity, purchased from Kunshan Ultrasonic Instrument Co., Ltd.) for 30 min. The hot suspension of sonicated Al-Fe_2O_3 nanothermite was then immediately added to the above estane-modified RDX suspension and ultrasonicated for 15 min. Afterward, the resulting brown product was filtered and vacuum-dried in an oven at 60 °C for 2 h.

The morphologies and surface appearances of the samples were characterized using field emission scanning electron microscopy (FESEM, Ultra-55, Carl Zeiss). The element distribution on the surface of the quasi-core/shell structure was characterized using X-ray photoelectron spectroscopy (XPS, VG ESCALAB 250).

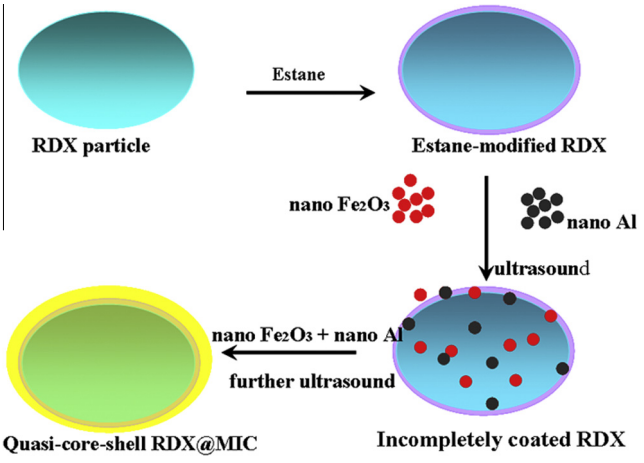

Fig. 1. Schematic for formation of quasi-core/shell structured RDX@Fe_2O_3–Al microparticle.

2.2. Measurement of combustion in a closed vessel

The pressure–time relation of the synthesized energetic material was determined by measuring the generated pressure in a closed vessel during combustion as a function of time. Fig. 2 shows the experimental setup for the pressurization measurement. For each test, loose powders with the same amount of R-RDX or F-RDX (60 mg) were loaded into a closed vessel with a volume of 1.0 cm^3. The pressure of the closed vessel was measured using a piezoelectric sensor with a pressure limit of 800 MPa, a response frequency of 400 kHz, and a rise time of 2 μs. The time-pressure curve was generated through data processing based on an amplifier and an oscilloscope.

2.3. Measurement in DDT tube

The DDT was measured using a classical DDT-tube [36], as shown in Fig. 3. A steel tube with thickness of 5 mm, inner diameter of 8 mm, and length of 300 mm was used for confinement during the DDT of the RDX@Fe_2O_3–Al composites. Ionization pins were used for time recording with a spacing of 10 mm, and the ionization pin signals were detected with a digital oscilloscope. For each test, the RDX@Fe_2O_3–Al powders were loaded at a low density of 0.54 g/cm^3 to 0.60 g/cm^3 and ignited with a igniter with length of 10 mm. To save the RDX@Fe_2O_3–Al samples, cotton was inserted into the tube near the plug where the detonation would have occurred and lasted for a certain distance, as shown in Fig. 3(a). In this method, DDT was not disturbed, and the detonation quenching could be observed in this area. The positions and distances of the ionization pins and igniter were recorded before each test. The corresponding times of shock wave propagation were recorded using a digital oscilloscope connected to a computer.

2.4. Sensitivity tests

The performed mechanical sensitivity tests were similar to those reported in the literature [37]. For comparison, dinitrodiazophenol (DDNP), a commonly used PE was tested under the same conditions. The impact sensitivity was tested using a drop hammer apparatus with a standard method. Around 30 mg of the sample was placed between steel anvils and hit by a 2.0 kg hammer that was dropped from a height of 25 cm. Twenty-five samples were tested. Initiation was defined as any evidence of flash, flame, or explosion that occurred upon impact. The explosion probability (P) was used as an indicator for impact sensitivity, as a higher P would result in a higher impact sensitivity value. The friction sensitivity was determined utilizing a WM-1 pendulum friction apparatus. The test was performed with a standard method.

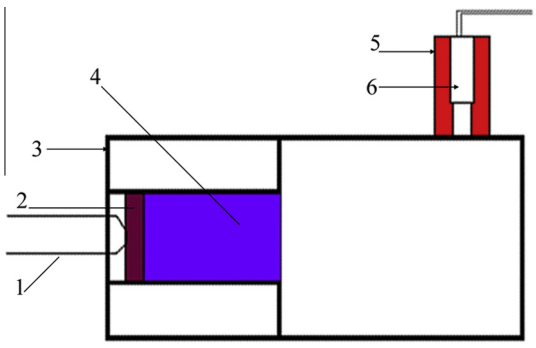

Fig. 2. Schematic of the experimental setup of closed vessel combustion measurements: (1) electric wire, (2) igniter, (3) metal support, (4) test sample, (5) pressure sensor holder, and (6) pressure sensor.

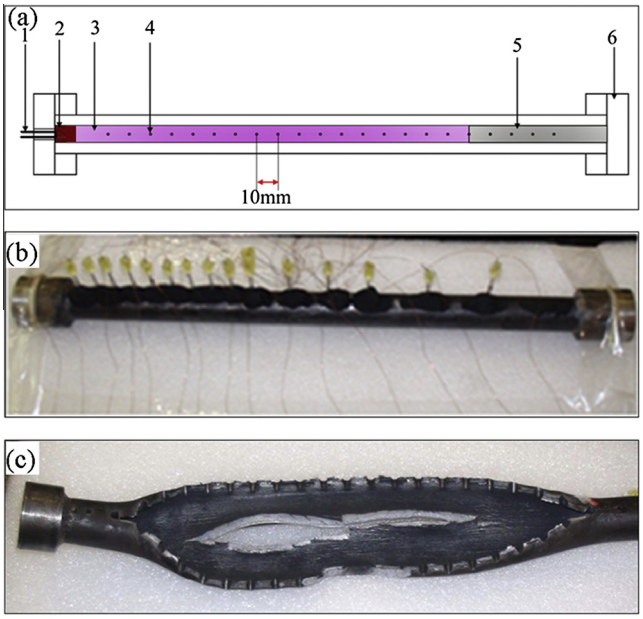

Fig. 3. (a) Schematic of DDT-tube: (1) electric wire, (2) igniter, (3) test material, (4) ionization pins, (5) cotton, and (6) plug; (b) photo of DDT-tube before ignition, and (c) photo of DDT-tube after experiment.

Twenty (20) mg of sample was placed between steel anvils and hit by a 1.5 kg pendulum hammer fixed at a 60° tilt angle. The gauge pressure showed a 0.88 MPa reading. Twenty-five samples were tested. The friction sensitivity was also expressed by P. The greater the P is, the higher the friction sensitivity is.

The ES sensitivity analyses of the F-RDX, DDNP, and F-RDX@Fe_2O_3–Al-nanothermites were performed using an electrical instrument service electrostatic discharge tester similar to that reported in the literature [38]. The distance between the electrodes was 0.5 mm, and a charging capacitor with capacitance of 30 μF was adopted. In each test, 20 mg of each sample was loaded, and the ES threshold was defined as E_{50} according to the standard up–down experimental procedure. As E_{50} increases, the ES sensitivity decreases.

3. Results and discussion

3.1. Structure characterizations

Two kinds of RDX with different particle sizes are used to discuss the effects of core particle size on the combustion and DDT of the quasi-core/shell structure. The R-RDX particles shown in Fig. 4(a) are mainly gem-like in shape with smooth surfaces and the particle sizes are around 25–75 μm. After treating with Fe_2O_3–Al nanothermites, the R-RDX particles exhibit rough surfaces (Fig. 4(c)), and the close-up view (inside image of Fig. 4(c)) shows that the RDX surface at the microscale is completely enwrapped by fine nanothermite nanoparticles. However, the F-RDX particles have irregular shapes with partial aggregation, as shown in Fig. 4(b), and their diameters are within 1–5 μm. After treating with Fe_2O_3–Al nanothermites, most F-RDX particle surfaces become covered with nanothermites (Fig. 4(d)).

Fig. 5 shows the elemental composition of the composite particle surfaces determined through XPS. For the RDX@Fe_2O_3–Al composite, only Fe, and Al could be found in the Fe_2O_3–Al nano-thermites, and only N element could be detected in RDX. Therefore, we could analyze the composite microstructure through the intensities and distributions of these elements on the surface.

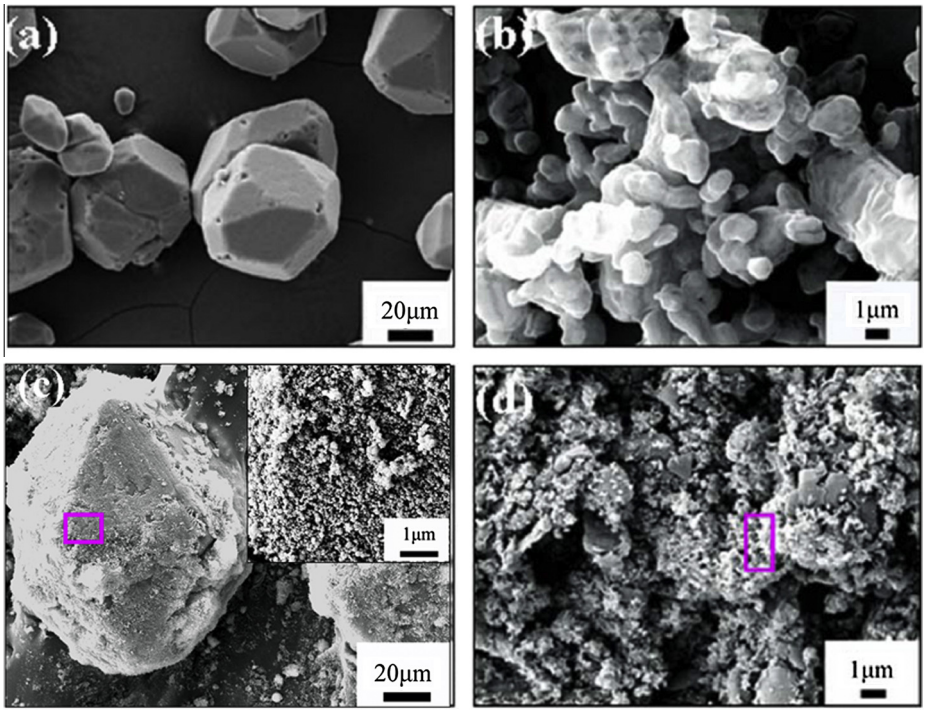

Fig. 4. SEM images of RDX@Fe_2O_3–Al composites: (a) R-RDX, (b) F-RDX, (c) R-RDX@Fe_2O_3–Al (70%/30%), and (d) F-RDX@Fe_2O_3–Al (70%/30%).

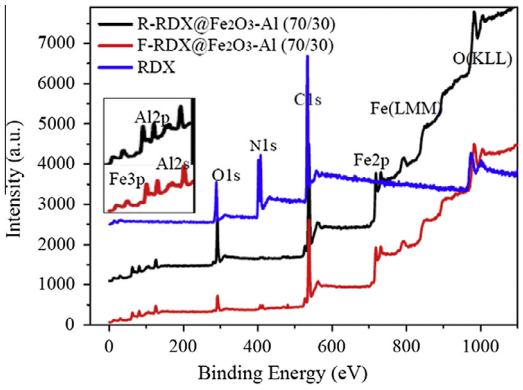

Fig. 5. XPS patterns of RDX@Fe_2O_3–Al-nanothermite composite.

From the results, Al2p, Al2s, Fe3p, and Fe2p peaks with binding energies of 30, 60, 80, and 730 eV, respectively, were detected in the R-RDX@Fe_2O_3–Al and F-RDX@Fe_2O_3–Al composites, but are absent in RDX. More importantly, N1s in RDX with binding energy around 405 eV completely disappeared in R-RDX@Fe_2O_3–Al, indicating that the R-RDX surface is completely enwrapped by Fe_2O_3–Al nano-thermites forming a core/shell structure. With this structure, the R-RDX core is not detected through XPS. Although the N1s of the F-RDX@ Fe_2O_3–Al composite could still be detected through XPS, the peak intensity is substantially weak and could be hardly observed. These results well agree with SEM results, and could be explained through the different surface areas of the RDX core between the R-RDX@Fe_2O_3–Al and F-RDX@Fe_2O_3–Al composites. The latter need more Fe_2O_3–Al-nanothermite particles to form a whole core–shell structure. From the XPS patterns, C1s near 532 eV appeared in all the samples because the impurities in Fe_2O_3 are not completely removed during thermal processing. Therefore, the quasi-core/shell structure, with RDX as the core and Fe_2O_3–Al nano-thermites as the shell, are forming through surface modification and ultrasonic enwrapping.

3.2. Combustion in closed vessel

To determine the combustion acceleration of the quasi-core/shell structured materials, the pressure–time relation of the F-RDX@Fe_2O_3–Al and R-RDX@Fe_2O_3–Al composites in closed-vessel combustion experiment is measured, and the corresponding pressure vs. time curves are shown in Fig. 6. For comparison, the mixtures of RDX and Fe_2O_3 nanoparticles are also measured having the same mass ratio to distinguish the surface ignition enhancement of Fe_2O_3–Al by the Fe_2O_3 catalysis. The pressure rapidly increases during the reaction propagation until the maximum pressure (P_{max}) reached, and then it slowly decreases with time in a closed vessel combustion. In this study, the pressure increasing time (PIT) is defined as time length necessary for a pressure rise from 10% to 90%, and the average pressurization rate (APR) is described as the quotient as the pressure differential is divided by PIT.

Table 1 and Fig. 6(a) show that the P_{max} increases when Fe_2O_3–Al or Fe_2O_3 added into F-RDX. The P_{max} is 130 MPa when 100% F-RDX combustion, while when 30% Fe_2O_3, 30% Fe_2O_3–Al, and 50% Fe_2O_3–Al added into F-RDX, the P_{max} increases to 134 MPa, 138 MPa, and 139 MPa respectively. This increase could contribute to the rapid combustion propagation and is in agreement with results reported in the literature [39]. As expected, evident combustion acceleration is observed when 30% Fe_2O_3 is added into F-RDX. PIT decreases from 248 μs to 230 μs, and the corresponding APR value increases from 0.429 MPa/μs to 0.466 MPa/μs. The results could be attributed to weak catalytic effect of the Fe_2O_3 nanoparticles on the F-RDX decomposition.

The combustion velocity of the F-RDX composite enwrapped by 30% Fe_2O_3–Al is significantly higher than that of the F-RDX composite enwrapped by 30% Fe_2O_3. The F-RDX/Fe_2O_3–Al PIT value decreases from 230 μs to 142 μs, and the F-RDX/Fe_2O_3–Al APR value increases from 0.466 MPa/μs to 0.777 MPa/μs. Moreover, similar results are in the combustion of the R-RDX, R-RDX@Fe_2O_3, and R-RDX@Fe_2O_3–Al composites. As the Fe_2O_3–Al nanothermite content increases, the surface ignition is enhanced, the APR value increases, and the corresponding PIT value decreases.

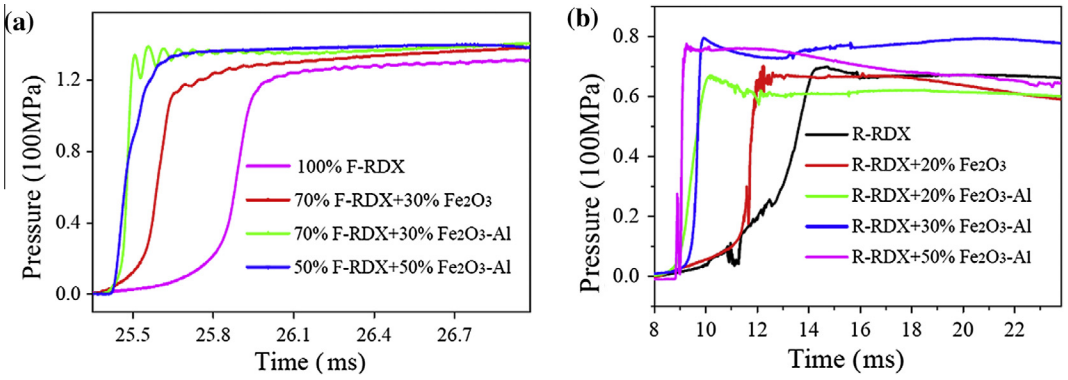

Fig. 6. Pressure vs. time curves during closed-vessel combustion of (a) F-RDX@Fe_2O_3–Al and (b) R-RDX@Fe_2O_3–Al.

Table 1
Pressure–time measurements of RDX@Fe_2O_3–Al composites in a closed-vessel.

Sample	PIT (μs)	P_{max} (MPa)	APR (MPa/μs)
100% F-RDX	248	130	0.429
70% F-RDX + 30% Fe_2O_3	230	134	0.466
70% F-RDX + 30% Fe_2O_3–Al	142	138	0.777
50% F-RDX + 50% Fe_2O_3–Al	44	139	2.527
100% R-RDX	4252	106	0.019
80% R-RDX + 20% Fe_2O_3	1370	107	0.062
80% R-RDX + 20% Fe_2O_3–Al	904	101	0.089
70% R-RDX + 30% Fe_2O_3–Al	382	119	0.249
50% R-RDX + 50% Fe_2O_3–Al	254	117	0.368

Table 1 shows the substantial influence of the particle size and surface ignition enhancement for F-RDX@Fe_2O_3–Al. The F-RDX@Fe_2O_3–Al APR values are significantly larger than those of R-RDX@Fe_2O_3–Al with same Fe_2O_3–Al content because a large portion of the F-RDX surface area is enwrapped by the Fe_2O_3–Al nanothermites. The APR values of F-RDX@Fe_2O_3–Al APR values significantly increase more rapidly than that of R-RDX@Fe_2O_3–Al with increasing Fe_2O_3–Al nanothermite content. Accordingly, the PIT values of F-RDX@Fe_2O_3–Al PIT values are considerably lower than that of R-RDX@Fe_2O_3–Al.

3.3. DDT in tube

The shock wave generated by acceleration of the burning front is a key factor in DDT [40]. Faster combustion velocities and pressurization rates are essential to form and strengthen the shock wave. Surface ignition enhancement caused by the enwrapped nanothermite is characterized through the distance-time relationship of DDT. Fig. 7(a) and (b) shows the distance-time relations of F-RDX@Fe_2O_3–Al, R-RDX@Fe_2O_3–Al, F-RDX@Fe_2O_3, and R-RDX@Fe_2O_3 measured in DDT tubes. Table 2 lists the corresponding run-to-detonation distances of different Fe_2O_3–Al nanothermite contents and RDX particle sizes during DDT.

The DDT for F-RDX without any additive is a lengthy process with a long run-to-detonation distance (9.5 cm), and the transition time (time of reaction wave propagation from first ionization probe (2.5 cm) to detonation point) reaches 2300 μs, as shown in Fig. 7(a). However, the combustion acceleration is enhanced when 20% Fe_2O_3 are added into F-RDX. The run-to-detonation distance decreases to 7.5 cm, and the transition time in DDT evidently decreases to about 450 μs. These results could be attributed to the catalytic effect of the Fe_2O_3 nanoparticles similar to the results of the closed vessel combustion experiment. Moreover, the run-to-detonation distance decreases to 4.5 cm, and the transition time decreases to about 160 μs after the Fe_2O_3–Al nanothermite replaces the Fe_2O_3 nanoparticles (both at 20%), which indicated that the combustion acceleration caused by Fe_2O_3–Al nanothermite is significantly more rapid than that caused by Fe_2O_3 nanoparticles. And furthermore, the left side of the DDT tube (ignition position) was severely damaged for relatively short distance, as shown in Fig. 3(c).

Fig. 7(b) and Table 2 show the effects of the RDX particle size and Fe_2O_3–Al nanothermite content during DDT. The run-to-detonation distances of the R-RDX composites are 1.0 cm longer than those of the F-RDX composites at the same concentrations (20% Fe_2O_3 and 20% Fe_2O_3–Al), and the transition times of the F-RDX composites is always shorter than those of the R-RDX composites. These results indicate that a rapid acceleration occurs in fine RDX particles with large surface areas. Another interesting aspect is that the run-to-detonation distance decreases from 4.5 or 5.5 cm to 2.5 cm as the Fe_2O_3–Al content increases from 20% to 30% (Fig. 7(b) and Table 2), and the corresponding transition time decreases from several hundred microseconds to the limit of detection. These changing trends are similar for both F-RDX and R-RDX composites. The differences of the run-to-detonation distances and transition times of the F-RDX and R-RDX composites at 30% Fe_2O_3–Al content are not observed in this experiment because the minimum distance that could be measured is only up to 2.5 cm (from the ignition wire to the first ionization probe, including the 1.0 cm-long igniter). The above results also indicate that DDT could accelerate to a near ideal level through nanothermites. The minimum initiating charge of the RDX@Fe_2O_3–Al composites are less than 0.45 g, and the practical F-RDX run-to-detonation distance of the Fe_2O_3–Al content at 30% content may be <1.5 cm. Although this value is slightly higher than the common PEs (i.e., the minimum DDNP initiating charge is less than 0.1 g), the RDX@Fe_2O_3–Al DDT is significantly close to those of the PEs. Therefore, the RDX@Fe_2O_3–Al composites are adequate for a primer used for the detonation wave output.

3.4. DDT acceleration mechanism

The combustion velocities of nanothermites range from 100 m/s to 2000 m/s in loose powder states under low pressures [2,41,42]. However, the combustion velocities of high explosives (HEs), such as RDX and HMX, are only several meters per second at the same states. For the quasi-core/shell structure shown in Fig. 8, the rapid combustion of the nanothermite shell would release significant amounts of heat that could lead to high temperatures on the HE surface. As a result, the time shift between ignition events at different locations is reduced.

In contrast, the reaction region length (d) of HEs dramatically increases. The HE surfaces in the reaction region are ignited, and the particles continuously burn towards the interior until the

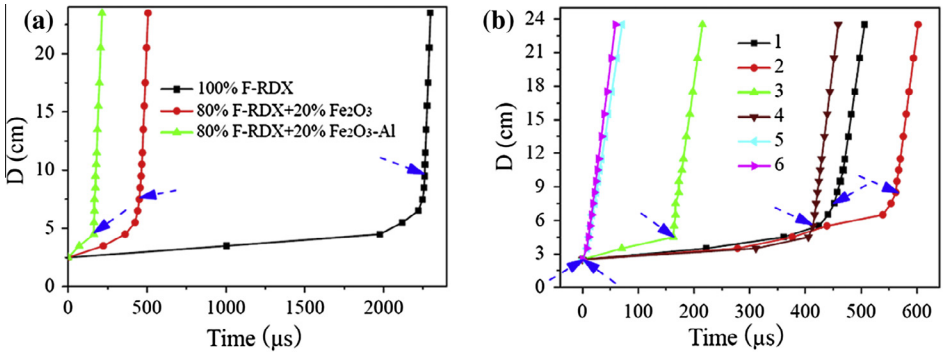

Fig. 7. Distance vs. time curves in DDT of composites. (a) F-RDX composites with different additions, (b) F-RDX and R-RDX composites with different additions: 1, 80% F-RDX + 20% Fe_2O_3; 2, 80% R-RDX + 20% Fe_2O_3; 3, 80% F-RDX + 20% Fe_2O_3–Al; 4, 80% R-RDX + 20% Fe_2O_3–Al; 5, 70% F-RDX + 30% Fe_2O_3–Al; 6, 70% R-RDX + 30% Fe_2O_3–Al.

Table 2
Comparison of run-to-detonation distances in DDT tests with different RDX particle sizes and Fe_2O_3–Al nanothermite contents.

Sample	Run distance (cm)
80% R-RDX + 20% Fe_2O_3	8.5
80% R-RDX + 20% Fe_2O_3–Al	5.5
70% R-RDX + 30% Fe_2O_3–Al	2.5
80% F-RDX + 20% Fe_2O_3	7.5
80% F-RDX + 20% Fe_2O_3–Al	4.5
70% F-RDX + 30% Fe_2O_3–Al	2.5

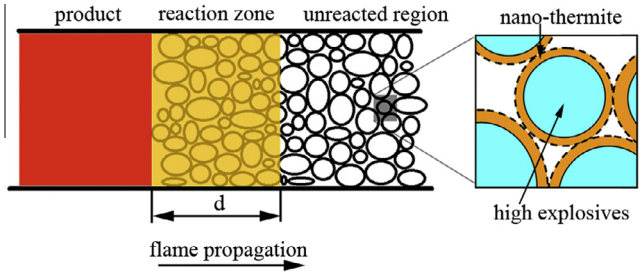

Fig. 8. Schematic for improving surface ignition and pressurization of HE particles via a quasi-core/shell structure.

Table 3
Sensitivities of F-RDX, DDNP, and F-RDX@ Fe_2O_3–Al composite.

Sample	Impact P (%)	Friction P (%)	ES E_{50} (mJ)
100% DDNP	72	92	28.7
100% F-RDX	8	0	132.7
70% F-RDX + 30% Fe_2O_3–Al	4	28	79.2

explosive particles are expended, and the reaction region is completely converted into gas products with high pressures. Compared with the porous energetic materials, composites with the quasi-core/shell structures have similar reaction behaviors. However, their differences depend on the "void", which is artificially engineered and filled with "self-propagating" nanothermites. Thus, the flame propagation at low pressures is mainly dependent on the combustion velocity of the nanothermite, rather than on the pressure generated by the high temperature HE gas products. Therefore, a high flame propagation velocity would be achieved at low pressures for this quasi-core/shell structure. However, a significant number of HE particles burn out at the enhanced reaction region, producing various gases with high temperatures and pressures. As a result, the DDT acceleration could be achieved through the combustion acceleration and rapid pressure increase.

3.5. Sensitivities

Table 3 presents the sensitivity test results for F-RDX, FRDX@Fe_2O_3–Al, and DDNP. In the impact sensitivity test, the P of F-RDX@Fe_2O_3–Al with a mass rate of 70/30 is only 4%, which is significantly close to the F-RDX, and considerably smaller than that of DDNP. Analogously, in the friction sensitivity test, the P of F-RDX@Fe_2O_3–Al with a mass ratio of 70/30 composite is only 28%, and substantially smaller than that of DDNP. The result indicates that the mechanical sensitivities of the RDX@Fe_2O_3–Al composites with quasi-core/shell structure retain the HE features in their cores. In the electric sparkle sensitivity test, the E_{50} of F-RDX is 132.7 mJ, and after 30% Fe_2O_3–Al nanothermite is added into F-RDX and the quasi-core/shell structure is formed, the E_{50} value decreases to 79.2 mJ. This result indicates that the F-RDX@Fe_2O_3–Al electric sparkle sensitivity increases compared with that of F-RDX, and this result could be attributed to the higher electric sparkle sensitivities of the nanothermites. However, the E_{50} of F-RDX@ Fe_2O_3–Al is still significantly higher than DDNP (28.7 mJ), indicating that F-RDX@ Fe_2O_3–Al is safer for electrostatic discharge.

4. Conclusions

To be safe, green, and heavy metal free, a rapid DDT acceleration strategy is developed through quasi-core/shell structure materials based on Fe_2O_3–Al nanothermites synthesized by an easy surface-modifying and ultrasonic synthesis technology. FESEM and XPS characterizations show that the surfaces of the R-RDX and F-RDX particles are enwrapped by Fe_2O_3–Al nanothermites, which serve as shells. In addition, the RDX particles serve as the core in the quasi-core/shell structure materials.

In the closed-vessel combustion test, the combustion acceleration caused by the Fe_2O_3–Al nanothermites is more rapid than that caused by Fe_2O_3. Evident changes in the particle size are observed during the combustion process, in which finer RDX particles accelerate the combustion acceleration. For F-RDX particles with an average diameter within 1–5 μm, the PIT value decreases from 248 μs to 44 μs with increasing Fe_2O_3–Al nanothermite content from 0% to 50%. Moreover, the corresponding APR value increases from 0.419 MPa/μs to 2.527 MPa/μs.

In the DDT tube test, the DDT acceleration caused by the Fe_2O_3–Al nanothermite is more rapid than that caused by Fe_2O_3. Evident particle size changes could also be observed during DDT, in which finer RDX particles accelerate DDT. For the F-RDX composites, the run-to-detonation distance decreases from 9.5 cm to 2.5 cm (with even smaller distance possible) with increasing Fe_2O_3–Al nanothermite content from 0% to 30%. Therefore, the DDT of F-RDX@Fe_2O_3–Al with a mass rate of 70/30 is accelerated to a PE level.

The results of impact, friction, and electric sparkle sensitivity tests show that the *P* of F-RDX@Fe_2O_3–Al with a quasi-core/shell structure at a mass rate of 70/30 is significantly lower than that of DDNP.

All the above results indicate that RDX@Fe_2O_3–Al is a rapid DDT energetic material and should be green and safe alternative for PEs.

Acknowledgments

This work was supported by the National Natural Science Foundation of China (Nos. 11002128, 11272292, 11172276, 11172275, 11372288), Science Foundation for Young Scientist of Sichuan Province (2012JQ0038), and the Open Project of State Key Laboratory Cultivation Base for Nonmetal Composites and Functional Materials (No. 11zxfk22) from Southwest University of Science and Technology.

References

[1] Yetter RA, Risha GA, Son SF. Metal particle combustion and nanotechnology. P Combust Inst 2009;32(2):1819–38.
[2] Pantoya ML, Granier JJ. Combustion behavior of highly energetic thermites: nano versus micron composites. Propell Explos Pyrot 2005;30(1):53–62.
[3] Kim SH, Zachariah MR. Enhancing the rate of energy release from nanoenergetic materials by electrostatically enhanced assembly. Adv Mater 2004;16(20):1821–5.
[4] Staley CS, Morris CJ, Thiruvengadathan R, Apperson SJ, Gangopadhyay K, Gangopadhyay S. Silicon-based bridge wire micro-chip initiators for bismuth oxide–aluminum nanothermite. J Micromech Microeng 2011;21(11):115015.
[5] Wu C, Sullivan K, Chowdhury S, Jian G, Zhou L, Zachariah MR. Encapsulation of perchlorate salts within metal oxides for application as nanoenergetic oxidizers. Adv Funct Mater 2012;22(1):78–85.
[6] Rossi C, Zhang K, Estève D, Alphonse P. Nanoenergetic materials for MEMS: a review. J Microelectromech S 2007;16(4):919–31.
[7] Dreizin EL. Metal-based reactive nanomaterials. Prog Energy Combust 2009;35(2):141–67.
[8] Jian G, Chowdhury S, Sullivan K, Zachariah MR. Nanothermite reactions: is gas phase oxygen generation from the oxygen carrier an essential prerequisite to ignition? Combust Flame 2013;160(2):432–7.
[9] Chen M, Zhang FS, Zhu J. Detoxification of cathode ray tube glass by self-propagating process. J Hazard Mater 2009;165(1–3):980–6.
[10] Wang Y, Zhu J. Preparation of lead oxide nanoparticles from cathode-ray tube funnel glass by self-propagating method. J Hazard Mater 2012;215–216:90–7.
[11] Jian G, Liu L, Zachariah MR. Facile aerosol route to hollow CuO spheres and its superior performance as an oxidizer in nanoenergetic gas generators. Adv Funct Mater 2013;23(10):1341–6.
[12] Yang Y, Wang P, Zhang Z, Liu H, Zhang J, Zhuang J, et al. Nanowire membrane-based Nanothermite: towards processable and tunable interfacial diffusion for solid state reaction. Sci Reportes 2013;3:1694.
[13] Zhou X, Xu D, Zhang Q, Lu J, Zhang K. Facile green in situ synthesis of Mg/CuO core/shell nanoenergetic arrays with a superior heat-release property and long-term storage stability. ACS Appl Mater Interfaces 2013;5(15):7641–6.
[14] Severac F, Alphonse P, Esteve A, Bancaud A, Rossi C. High-energy Al/CuO nanocomposites obtained by DNA-directed assembly. Adv Funct Mater 2012;22(2):323–9.
[15] Patel VK, Bhattacharya S. High-performance nanothermite composites based on aloe-vera-directed CuO nanorods. ACS Appl Mater Interfaces 2013;5(24):13364–74.
[16] Jian G, Feng J, Jacob RJ, Egan GC, Zachariah MR. Super-reactive nanoenergetic gas generators based on periodate salts. Angew Chem 2013;52(37):9743–6.
[17] Yan S, Jian G, Zachariah MR. Electrospun nanofiber-based thermite textiles and their reactive properties. ACS Appl Mater Interfaces 2012;4(12):6432–5.
[18] Zhang W, Yin B, Shen R, Ye J, Thomas JA, Chao Y. Significantly enhanced energy output from 3D ordered macroporous structured Fe_2O_3/Al nanothermite film. ACS Appl Mater Interfaces 2013;5(2):239–42.
[19] Feng J, Jian G, Liu Q, Zachariah MR. Passivated iodine pentoxide oxidizer for potential biocidal nanoenergetic applications. ACS Appl Mater Interfaces 2013;5(18):8875–80.
[20] Martirosyan KS, Wang L, Vicent A, Luss D. Synthesis and performance of bismuth trioxide nanoparticles for high energy gas generator use. Nanotechnology 2009;20(40):405609.
[21] Weismiller MR, Malchi JY, Yetter RA, Foley TJ. Dependence of flame propagation on pressure and pressurizing gas for an Al/CuO nanoscale thermite. Proc Combust Inst 2009;32(2):1895–903.
[22] Giles J. Green explosives: collateral damage. Nature 2004;427:580–1.
[23] Barsan ME, Miller A. Lead health hazard evaluation. National Institute for Occupational Safety and Health, Cincinnati, Ohio, HETA Report; 1996: 91-0346-2572.
[24] Klapőtke TM, Stierstorfer J. The CN7-anion. J Am Chem Soc 2009;131(3):1122–34.
[25] Göbel M, Karaghiosoff K, Klapötke TM, Piercey DG, Stierstorfer J. Nitrotetrazolate-2N-oxides and the strategy of N-oxide introduction. J Am Chem Soc 2010;132(48):17216–26.
[26] Zeng X, Gerken M, Beckers H, Willner H. Synthesis and characterization of Carbonyl Diazide, OC $(N_3)_2$. Inorg Chem 2010;49(20):9694–9.
[27] Tao GH, Twamley B, Shreeve JM. Energetic nitrogen-rich Cu (II) and Cd (II) 5, 5′-azobis (tetrazolate) complexes. Inorg Chem 2009;48(20):9918–23.
[28] Galvez-Ruiz JC, Holl G, Karaghiosoff K, Klapotke TM, Loehnwitz K, Mayer P, et al. Derivatives of 1, 5-diamino-1 H-tetrazole: a new family of energetic heterocyclic-based salts. Inorg Chem 2005;44(12):4237–53.
[29] Talawar MB, Agrawal AP, Asthana SN. Energetic co-ordination compounds: synthesis, characterization and thermolysis studies on bis-(5-nitro-2*H*-tetrazolato-*N*2) tetraammine cobalt(III) perchlorate (BNCP) and its new transition metal (Ni/Cu/Zn) perchlorate analogues. J Hazard Mater 2005;120(1–3):25–35.
[30] Talawar MB, Sivabalan R, Mukundan T, Muthurajan H, Sikder AK, Gandhe BR, et al. Environmentally compatible next generation green energetic materials (GEMs). J Hazard Mater 2009;161(2–3):589–607.
[31] Yao W, Shen C, Lu Y. Fe_3O_4@C@polyaniline trilaminar core-shell composite microsphere as separable adsorbent for organic dye. Compos Sci Technol 2013;87:8–13.
[32] Wang B, Liu C, Yin Y, Yu S, Chen K, Liu P, et al. Double template assisting synthesized core-shell structured titania/polyaniline nanocomposite and its smart electrorheological response. Compos Sci Technol 2013;86:89–100.
[33] Xia Y, Lu X, Zhu H. Natural silk fibroin/polyaniline (core/shell) coaxial fiber: fabrication and application for cell proliferation. Compos Sci Technol 2013;77:37–41.
[34] Tillotson TM, Gash AE, Simpson RL, Hrubesh LW, Satcher Jr JH, Poco JF. Nanostructured energetic materials using sol–gel methodologies. J Non-Cryst Solids 2001;285(1–3):338–45.
[35] Huang B, Hao X, Zhang H, Yang Z, Ma Z, Li H, et al. Ultrasonic approach to the synthesis of HMX@TATB core-shell microparticles with improved mechanical sensitivity. Ultrason Sonochem 2014;21(4):1349–57.
[36] Valiev DM, Bychkov V, Akkerman V, Eriksson LE. Different stages of flame acceleration from slow burning to Chapman–Jouguet deflagration. Phys Rev E 2009;80:036317.
[37] Li R, Wang J, Shen JP, Hua C, Yang GC. Preparation and characterization of insensitive HMX/graphene oxide composites. Propellants Explos Pyrot 2013;38(6):798–804.
[38] Weese RK, Burnham AK. Properties of CP: coefficient of thermal expansion, decomposition kinetics, reaction to spark, friction and impact. Propellants Explos Pyrot 2006;31(3):239–45.
[39] Thiruvengadathan R, Bezmelnitsyn A, Apperson S, Staley C, Redner P, Balas W, et al. Combustion characteristics of novel hybrid nanoenergetic formulations. Combust Flame 2011;158(5):964–78.
[40] Samirant M. DDT-determination of the successive phases of phenomena. Proceedings Ninth Symp (Int) on Detonation; 1989. p. 259.
[41] Dagaut P, Egolfopoulos FN. Editorial comment. Combust Flame 2012;159(1):1.
[42] Gan Y, Chen Z, Gangopadhyay K, Bezmelnitsyn A, Gangopadhyay S. An equation of state for the detonation product of copper oxide/aluminum nanothermite composites. J Nanopart Res 2010;12:719–26.